Journal of Molecular Spectroscopy 252 (2008) 31–36

Contents lists available at ScienceDirect

Journal of Molecular Spectroscopy

journal homepage: www.elsevier.com/locate/jms

High-resolution laser excitation spectroscopy of the $\widetilde{A}^2\Pi(000) - \widetilde{X}^2\Sigma^+(000)$ transition of BaOH

J.-G. Wang, J.D. Tandy, P.F. Bernath *

Department of Chemistry, University of York, Heslington, York YO10 5DD, England, UK

ARTICLE INFO

Article history:
Received 30 May 2008
Available online 21 June 2008

Keywords:
High-resolution
Laser excitation
BaOH

ABSTRACT

The high-resolution spectrum of the $\widetilde{A}^2\Pi(000) - \widetilde{X}^2\Sigma^+(000)$ transition of BaOH has been recorded using laser excitation spectroscopy. The BaOH molecules were synthesized through the reaction of Ba atoms with H_2O_2 in a Broida-type oven. Rotational and fine structure parameters have been determined for the $\widetilde{A}^2\Pi(000)$ state through a combined least-squares fit with the millimeter-wave pure rotational data of the $\widetilde{X}^2\Sigma^+$ state. The Λ-doubling constants observed for the $\widetilde{A}^2\Pi$ state are in poor agreement with the predictions of the pure precession model of the interactions between the $\widetilde{A}^2\Pi$ and the $\widetilde{B}^2\Sigma^+$ states of BaOH. In addition to the bands of the $\widetilde{A}^2\Pi(000) - \widetilde{X}^2\Sigma^+(000)$ transition, three bands located at ~11443 cm^{-1}, ~12013 cm^{-1} and ~12505 cm^{-1}, respectively, were also observed and analyzed but their vibrational and electronic assignments are not clear. Possible assignments of the three unidentified bands are discussed based on the derived spectroscopic constants and the vibrational assignments of previous low-resolution work.

1. Introduction

The spectroscopy of free radical alkaline earth monohydroxides has been a subject of interest since James and Sugden identified the colors in the emission from flames seeded with alkaline earth salts as the electronic transitions of alkaline earth monohydroxides [1]. In this group of molecules, CaOH [2–5] and SrOH [6–8] have been extensively studied using laser spectroscopy. Pure rotational analysis of several vibrational bands in the ground state of MgOH, CaOH and BaOH has been completed using millimeter-wave absorption spectroscopy by Ziurys et al. [9]. Transition frequencies and precise molecular constants have been derived from this analysis, which largely facilitate rotational analysis of excited electronic states. The first two excited electronic states, the $\widetilde{A}^2\Pi$ and $\widetilde{B}^2\Sigma^+$, of both CaOH [5] and SrOH [7,8] are good candidates for laser excitation spectroscopy because they are readily accessible using visible dye lasers. To access high-lying electronic states (>20000 cm^{-1}), optical–optical double resonance spectroscopy (OODR) has been proved to be a useful technique. Recently, Dick et al. [2] have rotationally analysed the $\widetilde{D}^2\Sigma^+$ (~28156 cm^{-1}) state of CaOH using OODR spectroscopy. Three high energy electronic states of SrOH, the $\widetilde{C}^2\Pi$ (~27307 cm^{-1}) [10], $\widetilde{B}'^2\Sigma^+$ (~26003 cm^{-1}) and $\widetilde{D}^2\Sigma^+$ (~27702 cm^{-1}) states [6] have also been investigated using this technique.

In comparison to CaOH and SrOH, spectroscopic investigations of BaOH have been relatively limited. The first high-resolution spectroscopic study of the $\widetilde{B}^2\Sigma^+ - \widetilde{X}^2\Sigma^+$ transition of BaOH was accomplished by Kinsey-Nielsen et al. in 1986 using laser excitation spectroscopy [11]. In this work, two vibrational bands, (000)–(000) and (001)–(000), of BaOH and one band, (000)–(000), of BaOD were rotationally analysed. The rotational analysis indicated that BaOH is a linear molecule in both the $\widetilde{X}^2\Sigma^+$ and $\widetilde{B}^2\Sigma^+$ states. An interesting observation in this work was that a separate set of spectroscopic constants were required for the *e*- and *f*-parity levels of the $\widetilde{B}$ state. Parity-dependent perturbations from $\widetilde{B}^2\Sigma^+ \sim \widetilde{A}^2\Pi$ interactions were proposed to rationalize this result. Following this work, Gustavsson et al. [12] further examined the $\widetilde{B}^2\Sigma^+ \sim \widetilde{A}^2\Pi$ local perturbations using 'perturbation selective' laser spectroscopy. A strong perturbation, which was believed to be from a vibronic Σ component of the $\widetilde{A}^2\Pi_{3/2}$ state, was observed in this work. The authors performed a deperturbation analysis but still failed to derive a common set of *e*/*f* constants for the $\widetilde{B}$ state.

The vibrational analysis of the $\widetilde{A}^2\Pi - \widetilde{X}^2\Sigma^+$ and $\widetilde{A}'^2\Delta - \widetilde{X}^2\Sigma^+$ transitions of both BaOH and BaOD were investigated using low-resolution laser excitation spectroscopy by Fernando et al. [13]. Band heads of the Ba–O–H bending and Ba–O stretching modes with v_2/v_3 up to 3 were determined. The spin–orbit splitting was found to be ~570 cm^{-1} for the $\widetilde{A}^2\Pi$ state. The two bands located at ~11784 and 11304 cm^{-1} were tentatively assigned to a stretching sequence of the $\widetilde{A}'^2\Delta_{5/2} - \widetilde{X}^2\Sigma^+$ transition. Pure rotational spectra of the $\widetilde{X}^2\Sigma^+$ state of BaOH/BaOD for three Ba isotopologues

* Corresponding author. Fax: +44 1904 432516.
E-mail address: pfb500@york.ac.uk (P.F. Bernath).

0022-2852/$ - see front matter © 2008 Elsevier Inc. All rights reserved.
doi:10.1016/j.jms.2008.06.006

were analyzed by Anderson et al. using millimeter-wave spectroscopy [14]. For higher-lying electronic states, Pooley et al. observed the $\widetilde{C}^2\Pi - \widetilde{X}^2\Sigma^+$ and $\widetilde{D}^2\Sigma^+ - \widetilde{X}^2\Sigma^+$ transitions using pulsed-dye laser excitation spectroscopy [15].

The $\widetilde{A}^2\Pi$ and $\widetilde{B}^2\Sigma^+$ states are believed to be correlated to the 6*p* and 5*d* atomic orbitals of Ba^+, and strong perturbations between the two states have been observed [11–13]. In order to more clearly understand these perturbations, a high-resolution study of the $\widetilde{A}^2\Pi$ state is obviously desirable. In the present paper we present the results of our high-resolution study of the $\widetilde{A}^2\Pi(000) - \widetilde{X}^2\Sigma^+(000)$ transition of BaOH using laser excitation spectroscopy. Rotational and fine structure constants have been determined for the $\widetilde{A}^2\Pi(000)$ state through a combined least-squares fit. The rotational analysis for three other bands in the range of the $\widetilde{A}^2\Pi(001) - \widetilde{X}^2\Sigma^+(001)$ and $\widetilde{A}^2\Pi(001) - \widetilde{X}^2\Sigma^+(000)$ transitions will also be presented. Perturbations between the $\widetilde{A}^2\Pi$ and $\widetilde{B}^2\Sigma^+$ states as well as possible perturbations from the $\widetilde{A}'^2\Delta_{3/2}$ state are also discussed.

2. Experimental

BaOH molecules were generated by the reaction of Ba metal vapour and H_2O_2 vapour in a Broida-type oven. Barium metal was resistively heated in an alumina crucible producing the metal vapour, which was then entrained in a flow of ~3 Torr of argon carrier gas. The reactant gas was introduced through a perforated ring above the crucible at ~5 mTorr, connected to a glass tube containing hydrogen peroxide. A chemiluminescent flame due to the production of the BaOH molecules was observed under optimal oven temperature and gas pressure conditions.

The $\widetilde{A}^2\Pi - \widetilde{X}^2\Sigma^+$ transition of BaOH was recorded by laser excitation spectroscopy. The output from a cw single-mode ring titanium:sapphire laser (Coherent 899-29) was focused vertically into the reaction chamber of the Broida oven. The typical laser power was ~450 mW. As the laser was scanned, the excitation fluorescence from the $\widetilde{A}^2\Pi$ state was collected using a photomultiplier tube (PMT). To simplify the observed spectra a 0.32 m monochromator was employed as a band-pass filter. When recording the spectrum of each band, the laser was first scanned to locate the appropriate band head. The laser was then fixed at the frequency of a band head while the monochromator was tuned in order to optimize the fluorescence signal. This monochromator position was then maintained while the laser was scanned through the required spectral range to obtain the high-resolution spectrum. The majority of bands obtained using this method were clear and easily assigned.

Phase sensitive detection was employed using a mechanical chopper to modulate the titanium:sapphire laser beam and a lock-in amplifier was used to process the fluorescence signal from the PMT. Spectra were recorded in 5 cm^{-1} segments at a scan speed of 2 GHz per second with a data sampling interval of 50 MHz. The absolute frequency of the laser was calibrated by simultaneously recording the absorption spectrum of a heated I_2 cell [16].

3. Results and analysis

In the previous low-resolution work, band heads at ~11 473 and 12 045 cm^{-1} were assigned to the $\widetilde{A}^2\Pi_{1/2}(000) - \widetilde{X}^2\Sigma^+(000)$ and $\widetilde{A}^2\Pi_{3/2}(000) - \widetilde{X}^2\Sigma^+(000)$ transitions, respectively [13]. Based on this vibrational assignment, high-resolution scans were performed. Fig. 1 shows an overview of high-resolution spectra of the $\widetilde{A}^2\Pi_{1/2}(000) - \widetilde{X}^2\Sigma^+(000)$ (top panel) and $\widetilde{A}^2\Pi_{3/2}(000) - \widetilde{X}^2\Sigma^+(000)$ (bottom panel) transitions plotted on a relative wavenumber scale in a spectral range of 85 cm^{-1}. Interestingly, as can be seen in Fig. 1, two band heads, denoted as U1 (~11 443 cm^{-1}) and U2 (~12 013 cm^{-1}) in the top and bottom spectrum respectively, also appeared in the same range. In addition to the four bands mentioned above, another band, at ~12 505 cm^{-1}, was also observed. This band was denoted as U3. With the exception of the band heads of the (000)–(000) and bands U1 and U2, some other head-like features (marked by asterisks) can also be observed in the spectra. It is possible that these bands originate from excited vibrational states of the $\widetilde{A}'^2\Delta - \widetilde{X}^2\Sigma^+$ transition [13]. Table 1 lists the band heads observed in this work.

The spectra of the two subbands in the $\widetilde{A}^2\Pi(000) - \widetilde{X}^2\Sigma^+(000)$ transition exhibit a Hund's case (a) $^2\Pi$—Hund's case (b) $^2\Sigma^+$ pattern with a clear $1B\ Q_{fe}/R_{ff}$ band head and the R_{ff}/Q_{fe} and P_{ee}/Q_{ef} pairs of branches [17]. The $3B\ R_{ee}$ branch head was also observed at ~11 506.810 cm^{-1} for the $\widetilde{A}^2\Pi_{1/2}(000) - \widetilde{X}^2\Sigma^+(000)$ transition as indicated in Fig. 1. The intensity distribution of the observed lines is affected by the position and bandwidth of the monochromator, as well as changes in the oven conditions as the laser scans.

Fig. 2 shows an expanded portion of the $\widetilde{A}^2\Pi_{1/2} - \widetilde{X}^2\Sigma^+$ transition spectrum of BaOH with the rotational assignments presented above. Both the P_{11}/Q_{12} and R_{12}/Q_{11} doublets due to the spin–rotation splitting in the $\widetilde{X}^2\Sigma^+$ state are fully resolved in this region. P_{12} lines are also discernable with a characteristic spacing of approximately three times the rotational constant, *B*. Fig. 3 illustrates the region of the BaOH spectrum corresponding to the R_{22}/Q_{21} branch head. The low-J'' and high-J'' rotational lines are congested because of the formation of the band head ($J'' \sim 34.5$ for R_{22} and $J'' \sim 35.5$ for Q_{21}). The R_{22}/Q_{21} paired lines start to be resolved at around $J'' = 14.5/15.5$, respectively.

The rotational (*J*) assignments of all the observed bands were made using lower state combination differences in the $\widetilde{X}^2\Sigma^+$ state [9]. 878 lines in the 12 branches of the $\widetilde{A}^2\Pi(000) - \widetilde{X}^2\Sigma^+(000)$ transition were assigned. The measured lines of the $\widetilde{A}^2\Pi(000) - \widetilde{X}^2\Sigma^+(000)$ transition were modelled using a standard Hund's case (a) $^2\Pi - {}^2\Sigma^+$ Hamiltonian [18]. A combined least-squares fit was performed, which included the 878 lines of the $\widetilde{A}^2\Pi(000) - \widetilde{X}^2\Sigma^+(000)$ transition (this work) and 47 pure rotational lines of the $\widetilde{X}^2\Sigma^+(000)$ state [9].

Rotational lines of all the six branches of the U2 band and five branches of the U1 band were assigned. The lines of the $3B\ R_{ee}$ branch of the U1 band fell in a congested spectral region and were not assigned. Although ambiguous electronic assignments for the upper states of the three bands, U1, U2 and U3 are an open problem at present, it is still possible to perform a least-squares fit using a Hund's case (c) state representation of the upper states of the U1, U2 and U3 bands. In particular, the rotational energy levels in a case (c) state were represented by the expression,

$$\begin{aligned} F(J) = {} & BJ(J+1) - D[J(J+1)]^2 + H[J(J+1)]^3 + L[J(J+1)]^4 \\ & \pm 1/2(J+1/2)[p + p_D(J+1/2)^2 + p_H(J+1/2)^4 \\ & + p_L(J+1/2)^6], \end{aligned} \quad (1)$$

where *B*, *D*, *H* and *L* are rotational constants and *p*, p_D, p_H and p_L are Ω-doubling constants. The ± sign refers to the *e*- (+) and *f*-parity (−) levels, respectively.

In the least-squares fits, each line was weighted according to its experimental uncertainty. For the millimeter-wave data [9] an estimated uncertainty of 10^{-6} cm^{-1} was adopted, while for the optical data of this work an uncertainty of 0.005 cm^{-1} was employed except for some overlapping lines (for which an uncertainty of 0.01 cm^{-1} was applied). Some effective higher order constants such as A_H, *H* and p_D were required to obtain a good fit of the measured spectral lines for the $\widetilde{A}^2\Pi(000) - \widetilde{X}^2\Sigma^+(000)$ transition. The spectroscopic constants generated from combined least-squares fits for the $\widetilde{X}^2\Sigma^+(000)$, $\widetilde{A}^2\Pi(000)$ and three unidentified electronic states are listed in Table 2. In this table, the three unidentified elec-

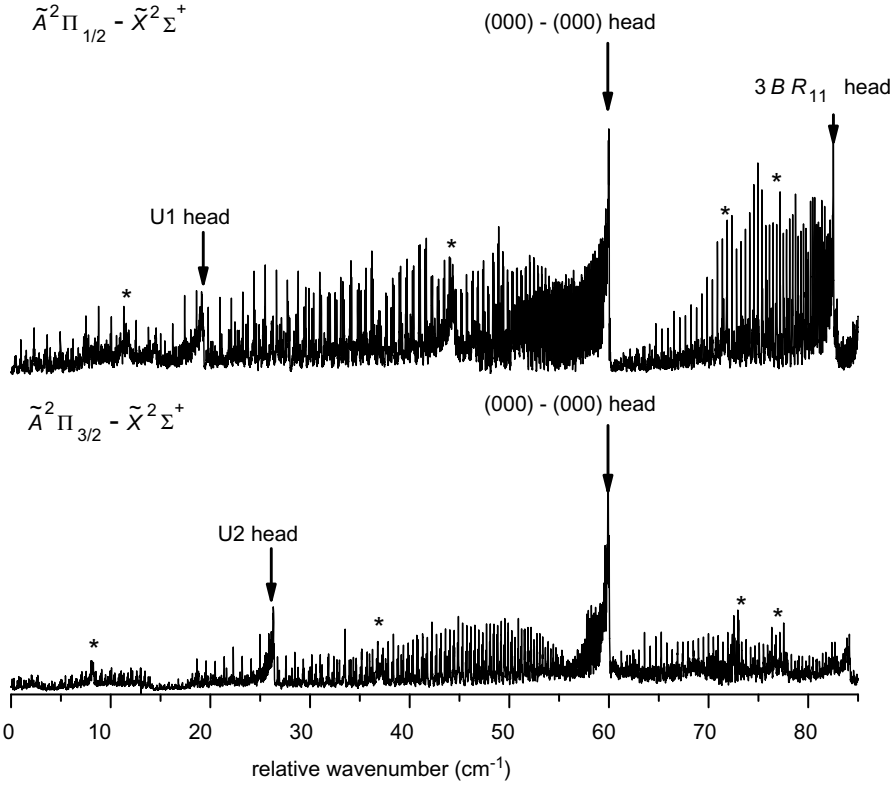

Fig. 1. The high-resolution laser excitation spectra of the $\tilde{A}^2\Pi_{1/2}(000) - \tilde{X}^2\Sigma^+(000)$ (top panel) and $\tilde{A}^2\Pi_{3/2}(000) - \tilde{X}^2\Sigma^+(000)$ (bottom panel) transitions of BaOH on a relative wavenumber scale in the spectral range of 85 cm^{-1}. The wavenumber zero for the $\tilde{A}^2\Pi_{1/2}(000) - \tilde{X}^2\Sigma^+(000)$ scan is 11424.3007 cm^{-1} while it is 11987.0014 cm^{-1} for the $\tilde{A}^2\Pi_{3/2}(000) - \tilde{X}^2\Sigma^+(000)$ panel. The spectra were recorded by scanning a single-mode ring titanium:sapphire laser and monitoring the fluorescence through a 0.32 m monochromator. The two spectra are aligned on the respective (000–000) branch heads of each transition. All six branches of each transition were observed and assigned. In addition to the two fundamental branch heads, two other bands (marked U1 and U2) were observed. Other head-like features (marked by asterisks) are likely to arise from the excited vibrational bands of the $\tilde{A}'^2\Delta - \tilde{X}^2\Sigma^+$ transition.

Table 1
Observed band heads (in cm^{-1})

Band head	Transition
11484.286	$\tilde{A}^2\Pi_{1/2}(000) - \tilde{X}^2\Sigma^+(000)$
12046.933	$\tilde{A}^2\Pi_{3/2}(000) - \tilde{X}^2\Sigma^+(000)$
11443.425	U1
12013.317	U2
12505.158	U3

tronic states are denoted as U_1, U_2 and U_3. The measured lines of all the observed bands are available as Supplementary material from this journal.

4. Discussion

The identification of the three bands U1 (~11443 cm^{-1}), U2 (~12013 cm^{-1}), and U3 (~12505 cm^{-1}) requires some consideration. The band head of the U2 band is consistent with the vibrational assignment of the $\tilde{A}^2\Pi_{3/2}(001) - \tilde{X}^2\Sigma^+(001)$ transition (~12010 cm^{-1}) in the low-resolution work [13]. The U2 band head is located at 34 cm^{-1} to the red of the R_{22}/Q_{21} head in the $\tilde{A}^2\Pi_{3/2}(000) - \tilde{X}^2\Sigma^+(000)$ transition. The search for a corresponding band for the $\tilde{A}^2\Pi_{1/2} - \tilde{X}^2\Sigma^+$ component yielded the band (U1) with a band head at ~11443 cm^{-1}, which was 41 cm^{-1} to the red of the R_{12}/Q_{11} head of the $\tilde{A}^2\Pi_{1/2}(000) - \tilde{X}^2\Sigma^+(000)$ transition. The $\tilde{A}^2\Pi(000)$ and the $\tilde{A}^2\Pi(001)$ states should have nearly identical spin–orbit splittings and thus the spectral intervals between the $\tilde{A}^2\Pi_{3/2}(000) - \tilde{X}^2\Sigma^+(000)$ and $\tilde{A}^2\Pi_{3/2}(001) - \tilde{X}^2\Sigma^+(001)$ heads (34 cm^{-1}) and the corresponding $\tilde{A}^2\Pi_{1/2}(000) - \tilde{X}^2\Sigma^+(000)$ and $\tilde{A}^2\Pi_{1/2}(001) - \tilde{X}^2\Sigma^+(001)$ heads (41 cm^{-1}) should be similar. This was not the case and no other bands were found in the region around 11450 cm^{-1}, the presumed band head position of the $\tilde{A}^2\Pi_{1/2}(001) - \tilde{X}^2\Sigma^+(001)$ component.

The rotational analysis provided some clues as to the identity of the U1, U2 and U3 bands. The least-squares fit for the assigned rotational lines of the U1 and U2 bands could only be made with the pure rotational frequencies of the $\tilde{X}^2\Sigma^+(001)$ state. In contrast, the least-squares fit for the U3 band required pure rotational frequencies of the $\tilde{X}^2\Sigma^+(000)$ state [9]. It is clear that the transitions of the U1 and U2 bands have a common lower state of $\tilde{X}^2\Sigma^+(001)$ and the U3 band has $\tilde{X}^2\Sigma^+(000)$ as its lower state.

The U3 band (~12505 cm^{-1}) falls in the spectral range of the $\tilde{A}^2\Pi_{3/2}(001) - \tilde{X}^2\Sigma^+(000)$ transition based on the Ba–O stretching frequency of 458 cm^{-1} in the $\tilde{A}^2\Pi$ state as reported in Ref. [13]. If this band can be identified as the $\tilde{A}^2\Pi_{3/2}(001) - \tilde{X}^2\Sigma^+(000)$ transition, then the $\tilde{A}^2\Pi_{1/2}(001) - \tilde{X}^2\Sigma^+(000)$ transition should be located near 11942 cm^{-1}. A high-resolution scan in this range resulted in an extremely congested spectrum that could not be assigned. Therefore, we cannot be certain that the U3 band is the $\tilde{A}^2\Pi_{3/2}(001) - \tilde{X}^2\Sigma^+(000)$ transition because its counterpart, the $\tilde{A}^2\Pi_{1/2}(001) - \tilde{X}^2\Sigma^+(000)$ transition, was not located.

The molecular constants derived from the least-squares fits may provide some information on the identity of the unknown upper electronic state for the U1 band. As can be seen from Table 2, only a p_D (2.027×10^{-6} cm^{-1}) Ω-doubling constant is derived for the U_1 upper state from the least-squares fit. This is too small for a Λ-doubling parameter in a Hund's case (a) $^2\Pi_{1/2}$ state, which should have a large p value. Clearly, the U_1 upper state is not a $^2\Pi_{1/2}$ state.

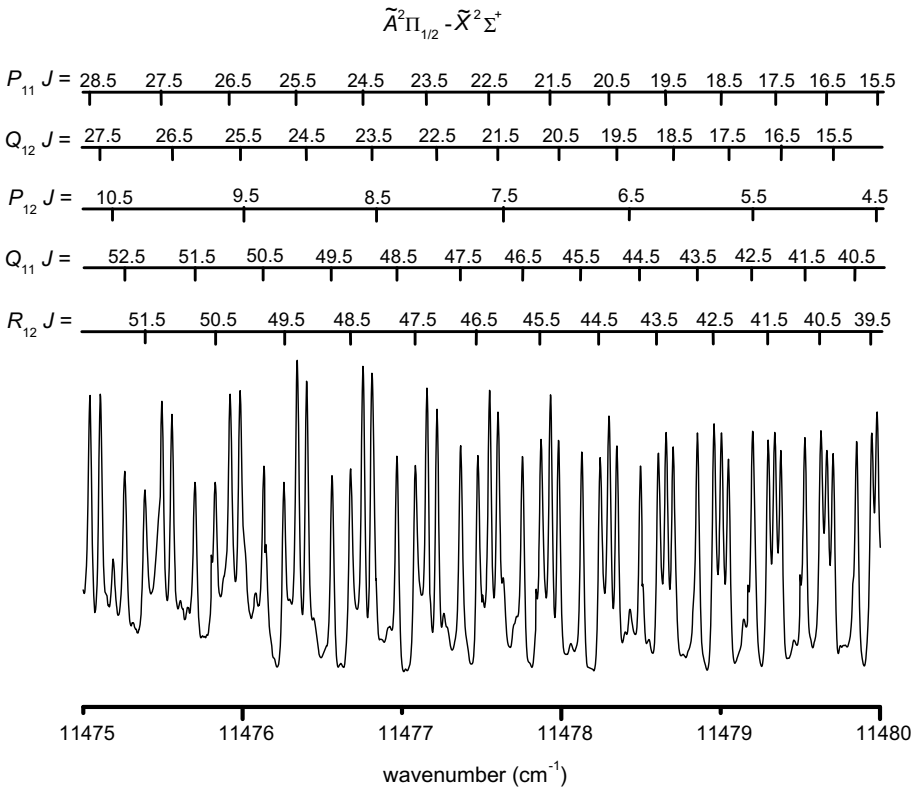

Fig. 2. An expanded portion of the laser excitation spectrum of the $\widetilde{A}^2\Pi_{1/2}(000) - \widetilde{X}^2\Sigma^+(000)$ transition of BaOH. J assignments of the P_{11}, Q_{12}, P_{12}, Q_{11} and R_{12} branches are presented above the spectrum. P_{11}/Q_{12} and R_{12}/Q_{11} doublets are split by the spin–rotation interaction in the ground state and are fully resolved in the illustrated region of the spectrum. The J values of the R_{12}/Q_{11} doublets increase with decreasing wavenumber in this region. P_{12} lines are also observed at lower intensities with a characteristic spacing of $\sim 3B$.

The band at $\sim$11 784 cm^{-1} observed in the low-resolution spectrum of BaOH was tentatively assigned to the $\widetilde{A}'^2\Delta_{5/2}(001) - \widetilde{X}^2\Sigma^+(000)$ transition by Fernando et al. [13]. A more likely assignment for this transition is $\widetilde{A}'^2\Delta_{5/2}(011) - \widetilde{X}^2\Sigma^+(000)$ because this transition becomes electronically allowed through vibronic coupling with the bending mode, similar to the $\widetilde{C}^2\Delta - \widetilde{X}^2\Sigma^+$ transition observed for CaOH [19]. Since the spin–orbit splitting of the $\widetilde{A}'^2\Delta$ state is not available for BaOH we may estimate it based on the value for BaF. The spin–orbit splitting of the $A^2\Pi$ state of BaF is approximately 11% larger than that of the $\widetilde{A}^2\Pi$ state of BaOH (632 cm^{-1} [20] versus 560 cm^{-1}, see Table 2). If a same ratio holds for the $A'^2\Delta$ state of BaF and the $\widetilde{A}'^2\Delta$ state of BaOH, a spin–orbit splitting of the latter may be estimated as $\sim$366 cm^{-1} [21], and the $\widetilde{A}'^2\Delta_{3/2}(012) - \widetilde{X}^2\Sigma^+(001)$ band should appear at $\sim$11 394 cm^{-1}. This estimated location does not agree with the U1 band origin of 11 441 cm^{-1} particularly well but it is not unacceptable considering the rough estimate of the spin–orbit splitting for the $\widetilde{A}'^2\Delta$ state of BaOH. It is therefore possible that the upper state of the U1 band is the $\widetilde{A}'^2\Delta_{3/2}(012)$ state. Some support for this assignment is obtained from the Ω-doubling constant, p_D, derived using the Hund's case (c) expression (1) for the U1 upper state. A $^2\Delta_{3/2}$ electronic state should have Λ-doubling that increases with J^3 (similar to a $^2\Pi_{3/2}$ state) but with a small Λ-doubling constant [22]. For a Hund's case (c) expression, the J^3 term belongs to the p_D constant and we derived a small value of $p_D = 2.027 \times 10^{-6}$ cm^{-1}.

The U2 band ($\sim$12 013 cm^{-1}) and the U3 band ($\sim$12 505 cm^{-1}) are located near the expected positions of the $\widetilde{A}^2\Pi_{3/2}(001) - \widetilde{X}^2\Sigma^+(001)$ transition and the $\widetilde{A}^2\Pi_{3/2}(001) - \widetilde{X}^2\Sigma^+(000)$ transition, respectively, according to the vibrational assignments of Ref. [13]. The upper states of the U2 and U3 bands have similar spectroscopic constants, but the two bands do not fit together if all of the lines are included. Due to the failure to find the corresponding $\widetilde{A}^2\Pi_{1/2} - \widetilde{X}^2\Sigma^+$ transitions, we are not able to unambiguously assign these bands. Another possibility is that the U2 and U3 bands also belong to the $\widetilde{A}'^2\Delta - \widetilde{X}^2\Sigma^+$ transition. For example, the $\widetilde{A}'^2\Delta_{5/2}(031) - \widetilde{X}^2\Sigma^+(001)$ transition would be observed at $\sim$11 976 cm^{-1}, which roughly agrees with the U2 band (12 013 cm^{-1}), based on the vibrational assignment and stretching and bending frequencies reported in Ref. [13]. A similar estimation may be made for the U3 band. As can be seen in Table 2, no Ω-doubling constant could be determined for the U2 upper state and only a small p_D derived for the U3 upper state.

In summary, it is possible that the U1 band is due to the $\widetilde{A}'^2\Delta_{3/2}(012) - \widetilde{X}^2\Sigma^+(001)$ transition and the U2 and U3 bands might have $\widetilde{A}^2\Pi_{3/2}(001)$ or $\widetilde{A}'^2\Delta$ upper states. Further work is needed to obtain more secure assignments for the U1, U2 and U3 bands.

Λ-doubling in the $\widetilde{A}^2\Pi$ state is well described by the 'pure precession' model [23] for many alkaline-earth halides and monohydroxides. The $\widetilde{A}^2\Pi$ and $\widetilde{B}^2\Sigma^+$ states form a unique perturber pair [24] with

$$p(\widetilde{A}^2\Pi) = \gamma(\widetilde{B}^2\Sigma^+) = \frac{2A_{SO}Bl(l+1)}{E(\widetilde{A}^2\Pi) - E(\widetilde{B}^2\Sigma^+)}, \quad (2)$$

and

$$q = \frac{2Bl(l+1)}{E(\widetilde{A}^2\Pi) - E(\widetilde{B}^2\Sigma^+)}, \quad (3)$$

where B is the rotational constant, A_{SO} is the spin–orbit constant, l is the atomic orbital angular momentum and E is the energy. For the case of SrOH, $A_{SO}(\widetilde{A}^2\Pi) \approx 264$ cm^{-1}, $B(\widetilde{A}^2\Pi) \approx 0.254$ cm^{-1},

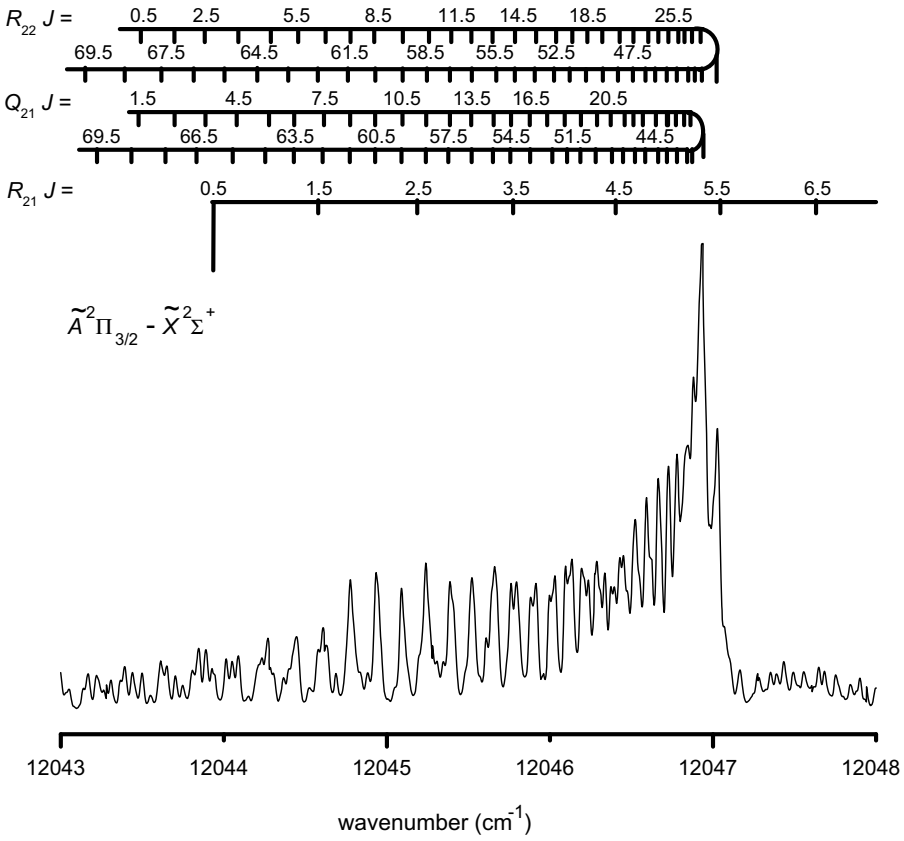

Fig. 3. An expanded portion of the laser excitation spectrum corresponding to the R_{22}/Q_{22} branch head of the $\tilde{A}^2\Pi_{3/2}(000) - \tilde{X}^2\Sigma^+(000)$ transition of BaOH. J assignments of the R_{21}, Q_{21} and R_{22} branches are presented above the spectrum. The formation of the band head at $J \sim 34.5$ for R_{22} and $J \sim 35.5$ for Q_{21} cause the low-J and high-J rotational lines to become congested in the illustrated region. These paired lines begin to be resolved at $\sim J = 14.5$ and 15.5 (R_{22} and Q_{21}, respectively).

Table 2
Spectroscopic constants (in cm^{-1}) for BaOH[a]

Constant	$\tilde{X}^2\Sigma(000)$[b]	$\tilde{X}^2\Sigma(001)$[c]	$\tilde{A}^2\Pi(000)$[b]	U_1[c]	U_2[c]	U_3[c]
T	0.0	0.0	11763.23628(32)	11441.2604(12)[e]	12009.8271(69)[e]	12502.54102(49)
B	0.2166092217(50)	0.215504482(57)	0.21235182(48)	0.2105571(32)	0.2123167(12)	0.21227958(96)
$D \times 10^{-7}$	1.642708(75)	1.64773(39)	1.6141(18)	1.879(22)	2.1267(39)	1.8198(41)
$H \times 10^{-13}$			−1.36(18)	4.87(37)		−4.63(40)
$\gamma \times 10^{-3}$	2.37943(47)	2.38243(75)				
$\gamma_D \times 10^{-9}$	7.57(35)					
A			560.10960(59)			
$A_D \times 10^{-3}$			2.40452(64)			
$A_H \times 10^{-8}$			−1.1946(65)			
$q \times 10^{-5}$			3.69(41)			
p			−0.146199(21)			
$p_D \times 10^{-6}$			−2.4888(53)	2.027(18)[d]		−1.387(14)[d]

[a] Values in parenthesis are 1σ standard deviations, in units of the last significant digits. U_1, U_2 and U_3 denote the upper electronic states corresponding the U1, U2 and U3 bands, respectively.
[b] Constants were generated by a combined fit of the $\tilde{A}^2\Pi - \tilde{X}^2\Sigma^+$ transition data and the millimeter-wave data of the $\tilde{X}^2\Sigma^+$ state [9] and a Hund's case (a) $^2\Pi$ Hamiltonian.
[c] Constants were derived from the combined fit of transition data of the U1, U2 and U3 bands and the millimeter-wave data of $\tilde{X}^2\Sigma^+$ [9] using a Hund's case (c) representation for the excited states.
[d] Effective Ω-doubling constant.
[e] Relative to the $\tilde{X}^2\Sigma^+(001)$ state.

$E(\tilde{A}^2\Pi) \approx 14674\ cm^{-1}$ [7], and $E(\tilde{B}^2\Sigma^+) \approx 16377\ cm^{-1}$ [8]; using an effective orbital angular momentum of $l = 1$ a value of p or γ is calculated as $\sim -0.157\ cm^{-1}$. The observed values of the $p(\tilde{A}^2\Pi)$ [7] and $\gamma(\tilde{B}^2\Sigma^+)$ [8] constants are, $-0.143296\ cm^{-1}$ and $-0.1447\ cm^{-1}$, respectively. It is clear that the interaction between the $\tilde{A}^2\Pi$ and $\tilde{B}^2\Sigma^+$ states is well modelled by the pure precession assumption.

For BaOH, we have $E(\tilde{B}^2\Sigma^+) \sim 13200\ cm^{-1}$ and $\gamma(\tilde{B}^2\Sigma^+) \sim -0.101\ cm^{-1}$ [11]. It should be noted that we have adopted the γ obtained from the P_{11}/R_{11} branches which has the biggest absolute value. Using the $E(\tilde{A}^2\Pi)$, $A_{SO}(\tilde{A}^2\Pi)$ and B values obtained in this work and an effective $l = 1$, from Eq. (2), we have

$$p(\tilde{A}^2\Pi) = \gamma(\tilde{B}^2\Sigma^+) \sim -0.333\ cm^{-1}.$$

The observed Λ-doubling constant of the $\tilde{A}^2\Pi$ state in this work, $p = -0.146199\ cm^{-1}$, is neither very close to the calculated value nor the spin-rotation constant of the $\tilde{B}^2\Sigma^+$ state. Moreover,

according to Eq. (3), the $\widetilde{A}^2\Pi$ state should have a negative q value, but our observed q value is $3.69 \times 10^{-5}\,\mathrm{cm}^{-1}$ (see Table 2). The pure precession model is obviously not very appropriate for the $\widetilde{B}^2\Sigma^+$ and $\widetilde{A}^2\Pi$ states of BaOH. More surprisingly the unique perturber approximation (i.e., $\gamma(\widetilde{B}^2\Sigma^+) \approx p(\widetilde{A}^2\Pi)$) is also not valid for BaOH.

A conflict between the observed and calculated p values and a positive constant q of the $A^2\Pi$ state was also observed for BaCl [25]. As there are no nearby $^2\Sigma$ states except the $B^2\Sigma^+$ state, the authors concluded that the non-validity of the pure precession approximation was partly due to the exclusion of possible perturbations from the near-lying $^2\Delta$ state [25]. We believe that the same argument should also be true in the case of BaOH. For both BaF and BaCl, the unique perturber approximation is still valid, but in BaOH there must be additional local vibronic perturbations to account for the fact that $\gamma(\widetilde{B}^2\Sigma^+) \neq p(\widetilde{A}^2\Pi)$.

It should be pointed out that the molecular constants listed in Table 2 need to be considered as 'effective' constants because of potentially strong local and global perturbations among the $\widetilde{A}^2\Pi$, $\widetilde{B}^2\Sigma^+$ and $\widetilde{A}'^2\Delta$ states. Strong mutual perturbations among the three states were observed for BaF and a deperturbation analysis was carried out [26,27].

5. Conclusions

The $\widetilde{A}^2\Pi(000) - \widetilde{X}^2\Sigma^+(000)$ transition of BaOH has been rotationally analyzed using laser excitation spectroscopy. Three other bands, denoted as U1 ($11\,143\,\mathrm{cm}^{-1}$), U2 ($12\,013\,\mathrm{cm}^{-1}$) and U3 ($12\,505\,\mathrm{cm}^{-1}$), have also been observed and rotationally assigned. The measured rotational lines were fitted in combination with the millimeter-wave pure rotational data of the $\widetilde{X}^2\Sigma^+$ state [9]. Rotational and fine structure constants have been determined for the $\widetilde{A}^2\Pi(000)$ state using the standard Hund's case (a) $^2\Pi$ Hamiltonian [18]. The assignments for the U1, U2 and U3 bands were discussed and spectroscopic constants were determined by fitting the assigned rotational lines to a Hund's case (c) energy level expression for the excited states. The lower states were determined as the $\widetilde{X}^2\Sigma^+(001)$ state for the U1 and U2 bands and the $\widetilde{X}^2\Sigma^+(000)$ state for the U3 band, but the upper states of the three bands could not be assigned with certainty. The pure precession and unique perturber models are not valid for the $\widetilde{B}^2\Sigma^+$ and $\widetilde{A}^2\Pi$ states of BaOH due to perturbations from the $\widetilde{A}'^2\Delta$ state. To make progress in understanding the nature of the low-lying electronic states of BaOH, an analysis of the $\widetilde{A}'^2\Delta$ state is required. The experiments are currently being prepared in our laboratory.

Acknowledgments

This research was supported by EPSRC. We thank S. Yu for providing some preliminary data on BaOH.

Appendix A. Supplementary data

Supplementary data for this article are available on ScienceDirect (www.sciencedirect.com) and as part of the Ohio State University Molecular Spectroscopy Archives (http://library.osu.edu/sites/msa/jmsa_hp.htm). Supplementary data associated with this article can be found, in the online version, at doi:10.1016/j.jms.2008.06.006.

References

[1] C.G. James, T.M. Sugden, Nature 175 (1955) 333–334.
[2] M.J. Dick, P.M. Sheridan, J.-G. Wang, S. Yu, P.F. Bernath, J. Mol. Spectrosc. 240 (2006) 238–243.
[3] R.A. Hailey, C. Jarman, P.F. Bernath, J. Chem. Phys. 107 (1997) 669–670.
[4] M. Li, J.A. Coxon, J. Chem. Phys. 104 (1996) 4961–4977.
[5] P.F. Bernath, C.R. Brazier, Astrophys. J. 288 (1985) 373–376.
[6] J.-G. Wang, M.J. Dick, P.M. Sheridan, S. Yu, P.F. Bernath, J. Mol. Spectrosc. 245 (2007) 26–33.
[7] C.R. Brazier, P.F. Bernath, J. Mol. Spectrosc. 114 (1985) 163–173.
[8] J. Nakagawa, R.F. Wormsbecher, D.O. Harris, J. Mol. Spectrosc. 97 (1983) 37–64.
[9] L.M. Ziurys, D.A. Fletcher, M.A. Anderson, W.L. Barclay Jr., Astrophys. J. Suppl. Ser. 102 (1996) 425–434.
[10] J.-G. Wang, P.M. Sheridan, M.J. Dick, P.F. Bernath, J. Mol. Spectrosc. 236 (2006) 21–28.
[11] S. Kinsey-Nielsen, C.R. Brazier, P.F. Bernath, J. Chem. Phys. 84 (1986) 698–708.
[12] T. Gustavsson, C. Alcaraz, J. Berlande, J. Cuvellier, J.-M. Mestdagh, P. Meynadier, P. De Pujo, O. Sublemontier, J.-P. Visticot, J. Mol. Spectrosc. 145 (1991) 210–221.
[13] W.T.M.L. Fernando, M. Douay, P.F. Bernath, J. Mol. Spectrosc. 144 (1990) 344–351.
[14] M.A. Aderson, M.D. Allen, W.L. Barclay Jr., L.M. Ziurys, Chem. Phys. Lett. 205 (1993) 415–422.
[15] S.J. Pooley, M.S. Beardah, A.M. Ellis, J. Electron. Spectrosc. Relat. Phenom. 97 (1998) 77–88.
[16] S. Gerstenkorn, J. Verges, J. Chevillard, Atlas du Spectre d'Absorption de la Molecule d'Iode, Laboratoire Aimé Cotton, CNRS II 91405 Orsay, France, 1982.
[17] G. Herzberg, Molecular Spectra and Molecular Structure, vol. 1, Krieger Publishing Company, Malabar, Florida, 1989.
[18] J.M. Brown, E.A. Colbourn, J.K.G. Watson, F.D. Wayne, J. Mol. Spectrosc. 74 (1979) 294–318.
[19] C.N. Jarman, P.F. Bernath, J. Chem. Phys. 97 (1992) 1711–1718.
[20] R.F. Barrow, M.W. Batin, B. Longborough, Proc. Phys. Soc. 92 (1967) 518–519.
[21] R.F. Barrow, A. Bernard, C. Effantin, J. D'Incan, G. Fabre, A. El Hachimi, R. Stringat, J. Vergès, Chem. Phys. Lett. 147 (1988) 535–537.
[22] J.M. Brown, A.S.-C. Cheung, A.J. Merer, J. Mol. Spectrosc. 124 (1987) 464–475.
[23] R.S. Mulliken, A. Christy, Phys. Rev. 38 (1931) 87–119.
[24] H. Lefebvre-Brion, R.W. Field, The Spectra and Dynamics of Diatomic Molecules, Elsevier, Amsterdam, 2004.
[25] G. Gustafsson, T. Gustavsson, H. Martin, J. Mol. Spectrosc. 131 (1988) 223–232.
[26] C. Effantin, A. Bernard, J. D'Incan, G. Wannous, J. Vergès, R.F. Barrow, Mol. Phys. 70 (1990) 735–745.
[27] A. Benard, C. Effantin, J. D'Incan, J. Vergès, R.F. Barrow, Mol. Phys. 70 (1990) 747–755.